• Clinical Research •

Novel mutation in *CNNM4* gene in a Chinese family with Jalili syndrome and literature review

Jing Lu, Si-Ying Liang, Zhi Li, Run Gan, Xiao-Rong Cheng, Qing-Shan Chen

Shenzhen Eye Hospital, Shenzhen Eye Medical Center, Southern Medical University, Shenzhen 518040, Guangdong Province, China

Correspondence to: Qing-Shan Chen. Shenzhen Eye Hospital, Shenzhen Eye Medical Center, Southern Medical University, 18 Zetian Road, Futian District, Shenzhen 518040, Guangdong Province, China. cqs1967@sina.com

Received: 2025-03-07 Accepted: 2025-04-28

Abstract

● **AIM:** To report two cases of Jalili syndrome (JS) harboring a novel mutation in the *CNNM4* gene, review previously published studies on JS, and analyze factors potentially associated with visual acuity in patients with JS.

● **METHODS:** Two JS patients from a non-consanguineous Chinese family underwent comprehensive ophthalmic evaluations. Next-generation sequencing (NGS) was performed to identify pathogenic variants, and Sanger sequencing was used for validation. A literature search was conducted to retrieve studies on JS published up to January 31, 2025; only studies with detailed records of visual acuity and mutation sites were included. Correlations between visual acuity and age, as well as between visual acuity and mutation domain, were analyzed.

● **RESULTS:** A total of 53 patients with detailed visual acuity and mutation site records from previous studies were included in the analysis. The mean logarithm of the minimum angle of resolution (logMAR) visual acuity was 1.15 (range: 0.69-2.00). Spearman's correlation analysis showed a positive correlation between visual acuity (logMAR) and age (r_s=0.502, P<0.001). No association was found between logMAR visual acuity and mutation domain (P=0.748). The 6-year-old proband and her 3-year-old brother carried a novel homozygous missense variant c.949A>C (p.Ser317Arg) in *CNNM4*. Both patients presented with reduced visual acuity, pendular nystagmus, photophobia, night blindness, color vision loss, macular atrophy, and amelogenesis imperfecta. Optical coherence tomography (OCT) revealed atrophy of the outer retinal layers, and electroretinography (ERG) showed extinguished cone and rod responses. Fundus autofluorescence (FAF) and fundus fluorescein angiography (FFA) of the proband demonstrated bilateral retinal pigment epithelium (RPE) defects around the optic disc, vascular arcades, and macular region. At the latest follow-up (30mo), the proband's condition remained stable: best-corrected visual acuity was 2.00 logMAR (right eye) and 1.30 (left eye), with no changes in fundus appearance. The younger brother had a best-corrected visual acuity of 1.52 logMAR in both eyes at the latest follow-up, accompanied by severe bilateral macular atrophy and obvious dentin discoloration due to progressive enamel thinning.

● **CONCLUSION:** This study reports a novel homozygous missense variant c.949A>C (p.Ser317Arg) in *CNNM4* in a Chinese JS family. Visual acuity in JS patients deteriorates with increasing age.

● **KEYWORDS:** Jalili syndrome; cone-rod dystrophy; amelogenesis imperfecta; *CNNM4*; visual acuity

DOI:10.18240/ijo.2025.12.18

Citation: Lu J, Liang SY, Li Z, Gan R, Cheng XR, Chen QS. Novel mutation in *CNNM4* gene in a Chinese family with Jalili syndrome and literature review. *Int J Ophthalmol* 2025;18(12):2354-2365

INTRODUCTION

Jalili syndrome (JS, OMIM # 217080), a rare autosomal-recessive genetic disease, was first described by Jalili and Smith[1] in Gaza in 1988. Later in 2009, the metal cation transport mediator 4 (*CNNM4*), residing at chromosome locus 2q11.2, was identified as the causative gene for JS[2-3]. Clinically, the two primary manifestations of JS are cone-rod dystrophy (CRD) and amelogenesis imperfecta (AI). CRD usually occurs in childhood or early adulthood with vision loss, nystagmus, photophobia, color-vision abnormalities, night blindness, bull's eye maculopathy, coloboma, and macular atrophy. Longitudinal evidence from a retrospective case series of JS demonstrated progressive worsening of retinal structure and function over time[4]. Histopathological study further revealed loss of retinal pigment epithelium (RPE), photoreceptors, and retinal ganglion cells in eyes of JS, with additional findings of abnormal dendritic arborization in bipolar and amacrine cells, disorganized Müller glia, and

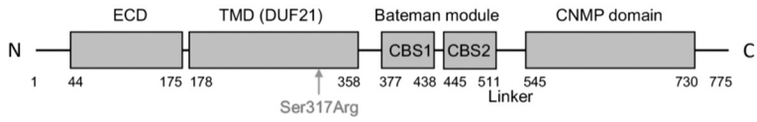

Figure 1 Schematic illustration of CNNM4 protein and the mutation site CNNM4 protein contains 4 domains: ECD, TMD (DUF21), CBS-pair domain, and CNMP domain. The arrow indicates the mutation site in the JS family. CBS: Cystathionine-β-synthase; CNMP: Cyclic nucleotide monophosphate; DUF: Domain of unknown function; ECD: Extracellular domain; JS: Jalili syndrome; TMD: Transmembrane domain.

activated microglia migrating to nuclear layers[5]. In parallel, AI manifests as defective dental enamel formation, typically affecting both primary and permanent dentitions. Affected individuals may exhibit yellowish or brown discoloration, surface pitting and roughness, irregular shapes, tooth loss, and anterior open bite (AOB) which is a form of malocclusion[6-7].

At the molecular level, the causative gene *CNNM4*, encoding a multidomain protein involved in the transport of magnesium ion (Mg^{2+}), is expressed in both neural retina and ameloblasts of developing teeth[2,8]. It has been hypothesized to be responsible for the removal of Mg^{2+} from these tissues. Mechanistically, loss-of-function mutations disrupt cellular Mg^{2+} extrusion, causing systemic hypomagnesemia and mineralization defects of tooth enamel due to Mg^{2+} accumulation[8-9]. Meanwhile, hypomagnesemia may induce oxidative stress and retinal cell apoptosis, causing retinal degeneration[10]. Structurally, CNNM4 protein contains four domains (Uniprot # Q6P4Q7, Figure 1): extracellular domain (ECD, 44-175)[11], transmembrane domain (TMD, 178-358)[7] also known as a domain of unknown function (DUF21), cystathionine-β-synthase (CBS)-pair domain (377-438 and 445-511), and cyclic nucleotide monophosphate binding-like (CNMP, 545-730) domain[12]. Between the two intracellular domains (CBS-pair and CNMP) lies a linker (512-544)[12]. Functional studies confirm that Mg^{2+}-ATP binding regulates CBS-pair domain to drive *CNNM4* dimerization[13] and Mg^{2+} efflux[14]. Of particular significance, CBS-pair deletion abolishes Mg^{2+} efflux[12], underscoring its essential role. CNMP domain can stabilize the conformational changes of CBS-pair domain[13], and is also required for *CNNM4* dimerization and Mg^{2+} efflux[15]. TMD cooperates with CBS-pair domain to mediate Mg^{2+} flux[16]. ECD is also essential for *CNNM4* dimerization and Mg^{2+} transport[11].

Despite these advances, genotype-phenotype correlations of JS remain poorly defined. We hypothesized that visual acuity decline may correlate with both aging and mutation location in functional domains. In the current study, we reported a JS case with a novel *CNNM4* mutation and reviewed previously reported JS cases up to January 31, 2025. We intended to summarize the reported visual acuity, clinical manifestations, and *CNNM4* mutations of JS, and analyze potential drivers of visual decline in these patients. This finding may guide prognostic counseling, while also underscoring the importance of longitudinal monitoring and implementation of low vision rehabilitation.

PARTICIPANTS AND METHODS

Ethical Approval The study was approved by the Institutional Review Board of Shenzhen Eye Hospital (Approval No. 2025KYPJ030). All procedures were conducted in accordance with the tenets of the Declaration of Helsinki and the informed consent was obtained from the patients' guardians.

Patients and Clinical Examination Two children diagnosed with JS in our hospital were from Wuchuan, Zhanjiang, Guangdong Province, China. Detailed medical and family histories were recorded. Two affected siblings had undergone detailed ophthalmic evaluations, including best corrected visual acuity (BCVA) using the decimal Snellen E chart, slit-lamp examination, dilated fundoscopy, optical coherence tomography (OCT; Carl Zeiss Meditec AG, Jena, Germany), electroretinogram (ERG), and color vision test (Ishsihara plates: 38-plate edition). Fundus autofluorescence and fundus fluorescein angiography (Spectralis HRA; Heidelberg Engineering, Heidelberg, Germany) were also performed on the proband. The OCT examination was performed using the radial scan pattern (12 B-scans, 9 mm length, centered on fovea).

Full-field ERGs were recorded using the handheld RETeval device (LKC Technologies, Gaithersburg, MD, USA). Its integrated infrared pupillometer continuously monitored pupil area (mm^2) during flicker stimulation, while stimulus intensity ($cd·s/m^2$) was synchronously recorded *via* LKC Technologies' acquisition software. The stimulus flash luminance ($cd·s/m^2$) was dynamically adjusted to maintain constant flash retinal illuminance (Td·s) according to the formula: flash retinal illuminance (Td·s)=flash luminance ($cd·s/m^2$)×pupillary area (mm^2). Protocols have been described previously[17-18], and followed the standard parameters of International Society for Clinical Electrophysiology of Vision[19]. In brief, patients were tested with natural pupils without dilation. Skin sensor strips were placed below the margin of the lower eyelid. After dark adaption for 20min, full-field scotopic rod responses to low intensity (0.01 $cd·s/m^2$) white light, scotopic maximal mixed rod-cone responses to bright light flash (3 $cd·s/m^2$), and scotopic oscillatory potentials (OPs) to bright light flash (3 $cd·s/m^2$) on a dark background were recorded. After light adaptation for 10min, photopic cone responses to bright light flash (3 $cd·s/m^2$), and flicker cone response were recorded.

Standard flicker cone parameters consist of 3.0 cd·s/m^2 (85 Td·s) white flashes on 30 cd/m^2 (848 Td) background with 28.306 Hz flicker stimulation[20-21]. All tests were performed in duplicate.

Genetic Testing Next-generation sequencing was used to identify the pathogenic variant, while Sanger sequencing was used for validation. Peripheral blood samples of the proband and her family were taken for genetic analysis after informed consent. Target region capture, sequencing, and data analysis were conducted by BGI Co., Ltd (Shenzhen, China). Genomic DNA was extracted with MagPure Buffy Coat DNA Midi KF Kit (Guangzhou Magen Biotechnology Co., Ltd, Guangzhou, China) according to the manufacturer's standard procedure. DNA library was built and sequenced with the MGISEQ-2000 high-throughput sequencing platform[22]. To detect the potential variants in the proband, bioinformatic processing and data analysis were performed after receiving the primary sequencing data. "Clean reads" were generated using previously published filtering criteria[23], and then aligned to the human genome reference[24]. Depth analysis of the genomic region, indels, and single-nucleotide variants in the selected gene panel for inherited ophthalmic diseases was performed. All single-nucleotide variants and indels were filtered and estimated *via* multiple databases, including NCBI dbSNP (build 155), HapMap 3, and 1000 Genomes (phase 3). The annotation source, dbNSFP (2.9.1), which contains seven well-established prediction programs, was used to predict the effect of missense mutation. The identified variant was assessed according to the protocol issued by the American College of Medical Genetics and Genomics[25]. The Human Gene Mutation Database (2022.3) was used to screen mutations reported in published studies. The mean depth of target regions was 365.37×, with a coverage rate of 99.83%. Absence of copy number variations was confirmed by analyzing the depth distribution of all mapped sequencing fragments. Segregation analyses in other family members were performed *via* conventional Sanger sequencing methods.

Search Strategy and Study Selection In order to study the possible factors associated with visual acuity, the databases of PubMed, Embase, and Web of Science were searched in order to identify all published studies concerning JS up to January 31, 2025. Among these studies, only those with detailed records of visual acuity and mutation site were included. Two investigators independently screened studies, with discrepancies resolved by a third reviewer. In order to analyze the association between visual acuity and mutation domain, three cases that carried mutations in more than one domain in CNNM4 protein were excluded to isolate domain-specific effects[4,26].

Statistical Analysis The relationship between visual acuity (as ordinal variable) and age in the JS patients was analyzed using Spearman's correlation. Normality of logarithm of the minimum angle of resolution (logMAR) data was confirmed using Shapiro-Wilk tests (P>0.05). The relationship between logMAR visual acuity (as scale variable) and domain was analyzed using simple linear regression. Statistical analysis was performed using SPSS version 26 (IBM, Armonk, NY, USA). A 2-tailed P value of less than 0.05 was considered statistically significant.

RESULTS

Clinical Findings There was no known history of parental consanguinity. The proband was a 6-year-old girl presented with reduced visual acuity, pendular nystagmus, and photophobia. On the initial visit at September 2022, her BCVA was 0.01 (corrected with +3.50/-2.25×178) in the right and 0.05 (corrected with +3.75/-2.25×178) in the left eye. The proband's affected brother was 3-year-old on his initial visit. He also presented with pendular nystagmus and photophobia. The affected siblings were absent of color vision, and suffered from impaired navigational abilities in dim light, indicating night blindness. They had normal anterior segments and pupillary reactions, but abnormal fundi. The fundi of the proband showed bull's eye maculopathy, attenuated retinal arteries, and retinal pigment epithelial mottling along the vascular arcades bilaterally (Figure 2A1, 2A2), which corresponded to the manifestations on autofluorescence and fluorescein angiography (Figure 3). Her fundus autofluorescence showed bilateral hypoautofluorescent areas around optic disc and vascular arcades, and an enlarged hypoautofluorescent area in the macular region, which correspond to the defect of retinal pigment epithelium (Figure 3A1, 3A2). Fundus fluorescein angiography revealed bilateral attenuated retinal vessels and mottled hyperfluorescence along the vascular arcades (Figure 3B-3D). A window defect was observed in the macular region of the right eye (Figure 3B1-3D1), and a blockage by pigmentation was seen in the macular region of the left eye (Figure 3B2-3D2). Spectral domain OCT of the proband revealed atrophy of the outer retinal layers, with absence of the photoreceptor layer (external limiting membrane, myoid zone, ellipsoid zone, photoreceptor outer segments, and interdigitation zone) and almost total loss of the outer nuclear layer bilaterally (Figure 2A3, 2A4). Full-field ERG of the proband showed flat waves for cone and rod responses, and impaired OPs bilaterally (Figure 4A). In addition to ocular abnormalities, she had dental decay, staining, irregular dentition, and AOB (Figure 5A1). As for the younger brother of the proband, he showed more profound macular atrophy and attenuated retinal arteries (Figure 2C1, 2C2). His dental abnormalities displayed as thin of enamel, pitting in the upper teeth, and AOB (Figure 5B1). He knocked out two front teeth by accident. No other systemic abnormality was found in these two patients. The older sister and parents of the proband were normal.

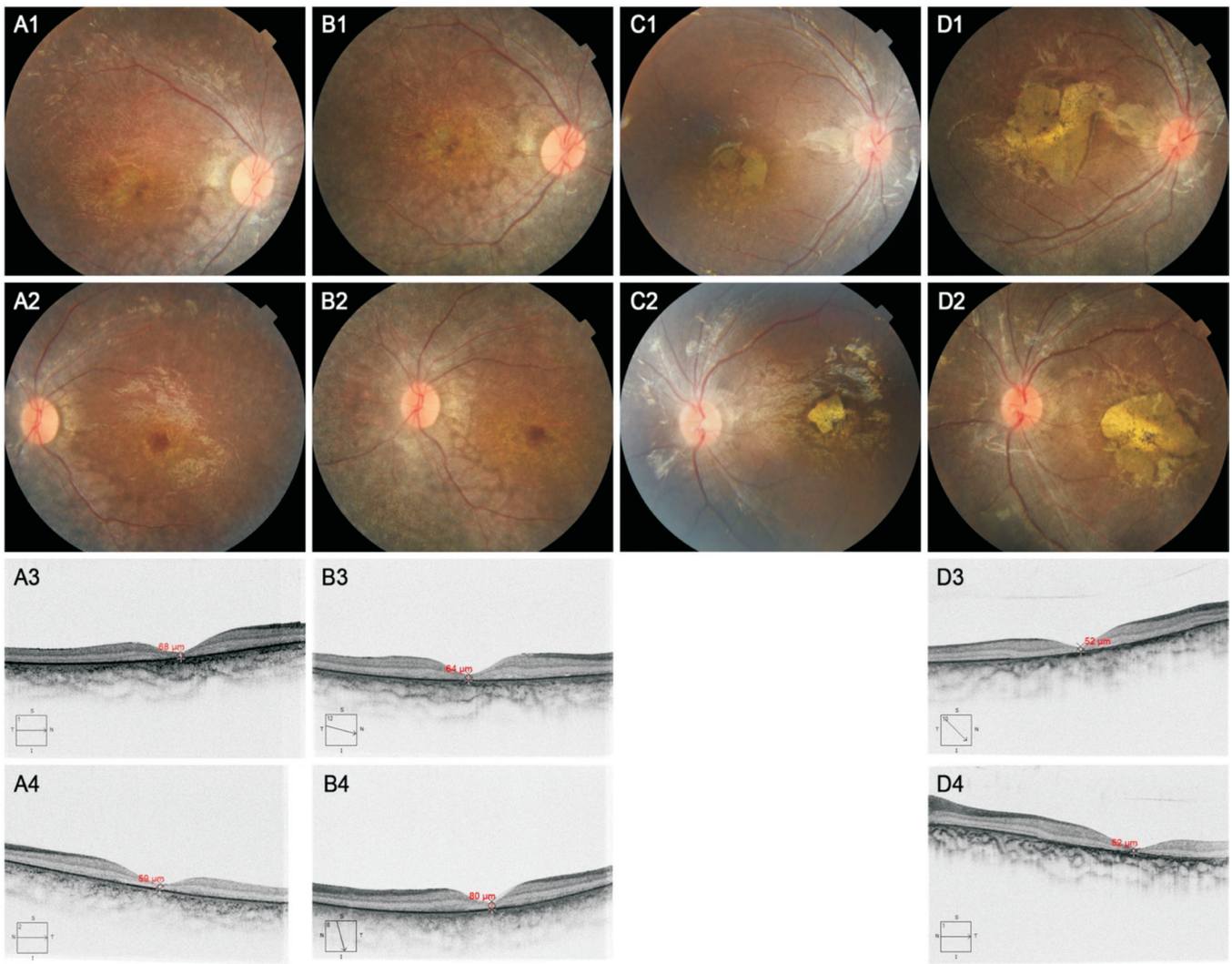

Figure 2 Multimodal retinal imaging of the proband and her sibling Color fundus photography of the proband showed bull's eye maculopathy, attenuated retinal arteries, and retinal pigment epithelial mottling along the vascular arcades in both eyes at the initial visit (A1 and A2). Spectral domain OCT of the proband revealed atrophy of the outer retinal layers, with absence of the photoreceptor layer and almost total loss of the outer nuclear layer bilaterally at the initial visit (A3 and A4). Her manifestations remained stable at 30mo follow-up visit (B1-B4). Color fundus photography of the youngest brother showed more profound macular atrophy bilaterally at the initial visit (C1 and C2). His macular atrophy extended more profoundly with pigmentation bilaterally at the latest follow-up visit 30mo later (D1 and D2). His macular fovea was extremely thin with absence of the photoreceptor layer, and part of the out nuclear layer remained in both eyes (D3 and D4).

On the latest visit at March 2025, the condition of the proband remained stable, with BCVA and fundus appearance remained unchanged (Figure 2B1-2B4). Her permanent teeth showed thin of enamel and irregular dentition (Figure 5A2). At this time, the proband's affected young brother was 5-year-old and could cooperate better with ocular examinations. His BCVA was 0.03 (corrected with +3.50/-3.50×9) in the right and 0.03 (corrected with +4.25/-3.50×178) in the left eye at the latest visit. His macular atrophy extended around with pigmentation bilaterally (Figure 2D1, 2D2). As shown by spectral domain OCT, although his macular fovea was extremely thin with absence of the photoreceptor layer, part of the out nuclear layer remained in both eyes (Figure 2D3, 2D4). Full-field ERG of him showed flat waves for cone and rod responses, and impaired OPs bilaterally (Figure 4B). Dentin color became apparent due to progressive enamel thinning (Figure 5B2). He lost another tooth in a fall.

Genetic Findings Next-generation sequencing along with Sanger sequencing identified a novel homozygous missense variant c.949A>C (p.Ser317Arg) in *CNNM4* in this JS family. The variant is located in the TMD of CNNM4 protein, as shown in Figure 1. Pedigree and *CNNM4* variant of the JS family were displayed in Figure 6. Two patients (II-2 and II-3) carried the same homozygous variant (C/C), and their parents (I-1 and I-2) carried the heterozygous variant (A/C). The healthy sister (II-1) carried the original homozygous A/A without mutation. According to guidelines of the American college of medical genetics and genomics, this variant was classified as a

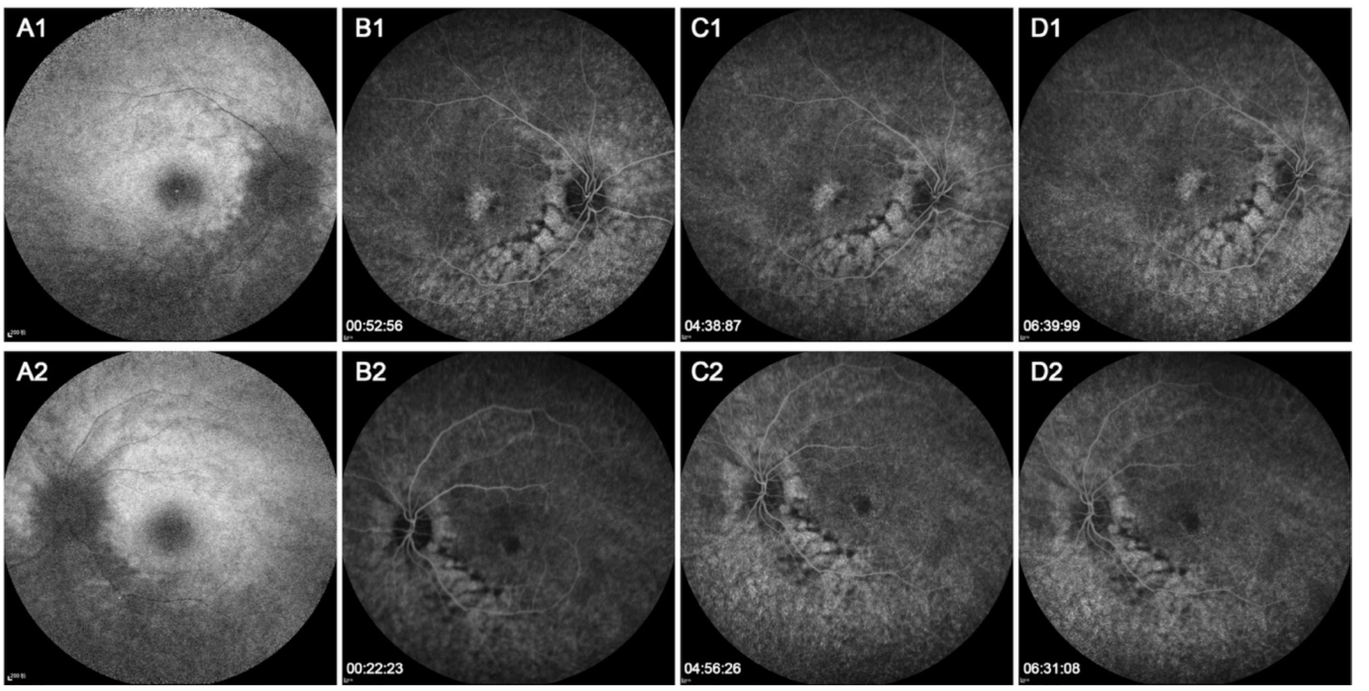

Figure 3 Fundus autofluorescence and fluorescein angiography of the proband Fundus autofluorescence showed hypoautofluorescent areas around optic disc, patchy hypoautofluorescence along the vascular arcades (more severe inferiorly), and an enlarged hypoautofluorescent area in the macular region that correspond to the defect of retinal pigment epithelium in both eyes (A1 and A2). Fundus fluorescein angiography demonstrated attenuated retinal vessels and mottled hyperfluorescence along the vascular arcades (window defect) with hypofluorescent streaks (pigmentation) bilaterally (B1-D1, B2-D2). A hyperfluorescent area resulted from window defect was observed in the macular region of the right eye (B1-D1), and a hypofluorescent patch resulted from blockage by pigmentation was seen in the macular region of the left eye (B2-D2).

variant of uncertain significance with the following evidence: PM2 (absent in population databases) and PM3_supporting (observed in trans with another likely pathogenic variant). The pathogenicity of this variant was predicted to be deleterious that might disrupt CNNM4 protein function by sorting intolerant from tolerant (SIFT).

Factors Associated with Visual Acuity In total, fifty three patients in previous papers with detailed records of visual acuity and mutation site were included in the analysis (Table 1). All visual acuities in fraction format were transformed into logarithm of the minimum angle of resolution (logMAR) format (n=40), while 13 cases with qualitative descriptions (*e.g.* light perception) were excluded from logMAR conversion. The mean logMAR visual acuity was 1.15, with a range of 0.69 to 2.00. In order to include visual acuity that was no better than finger count into analysis, visual acuity was classified according to the ICD-11 categories for vision impairment (https://icd.who.int/browse/2025-01/mms/en#1103667651): level 0 (no vision impairment: 6/12 or better), level 1 (mild vision impairment: 6/18 to worse than 6/12), level 2 (moderate vision impairment: 6/60 to worse than 6/18), level 3 (severe vision impairment: 3/60 to worse than 6/60), level 4 (blindness: 1/60 or counts fingers at 1 m to worse than 3/60), level 5 (blindness: light perception to worse than 1/60 or counts fingers at 1 m), level 6 (blindness: no light perception)[27]. The classified visual acuity and its corresponding age information were summarized in Table 2. Noted that visual acuity could deteriorated to level 5 with the minimum age of 15-year-old as reported so far.

Spearman's correlation analysis demonstrated that the visual acuity level (categorized by ICD-11) was positively associated with age (r_s=0.502, P<0.001), indicating that the visual acuity of JS patients deteriorated with aging. In addition, the relationship between logMAR visual acuity and mutation domain was analyzed using simple linear regression. In order to reduce the effects of age on the analysis, ANCOVA with age as a covariate was performed to isolate domain effects. Cases with mutation site on the linker was excluded due to its limited sample size (n=3). Finally, no relationship between logMAR visual acuity and mutation domain was detected (P=0.674, n=37). Since the number of the reported JS cases with detailed records of visual acuities and mutation sites was quite limited until present, analysis with larger sample size is warranted to validate this preliminary result in the future.

DISCUSSION

The present study reported a novel homozygous missense variant c.949A>C (p.Ser317Arg) in *CNNM4* in a Chinese family with JS. This variant was predicted to be deleterious by SIFT and the affected patients in the current study presented with typical features of JS. JS is a rare oculo-dental disorder

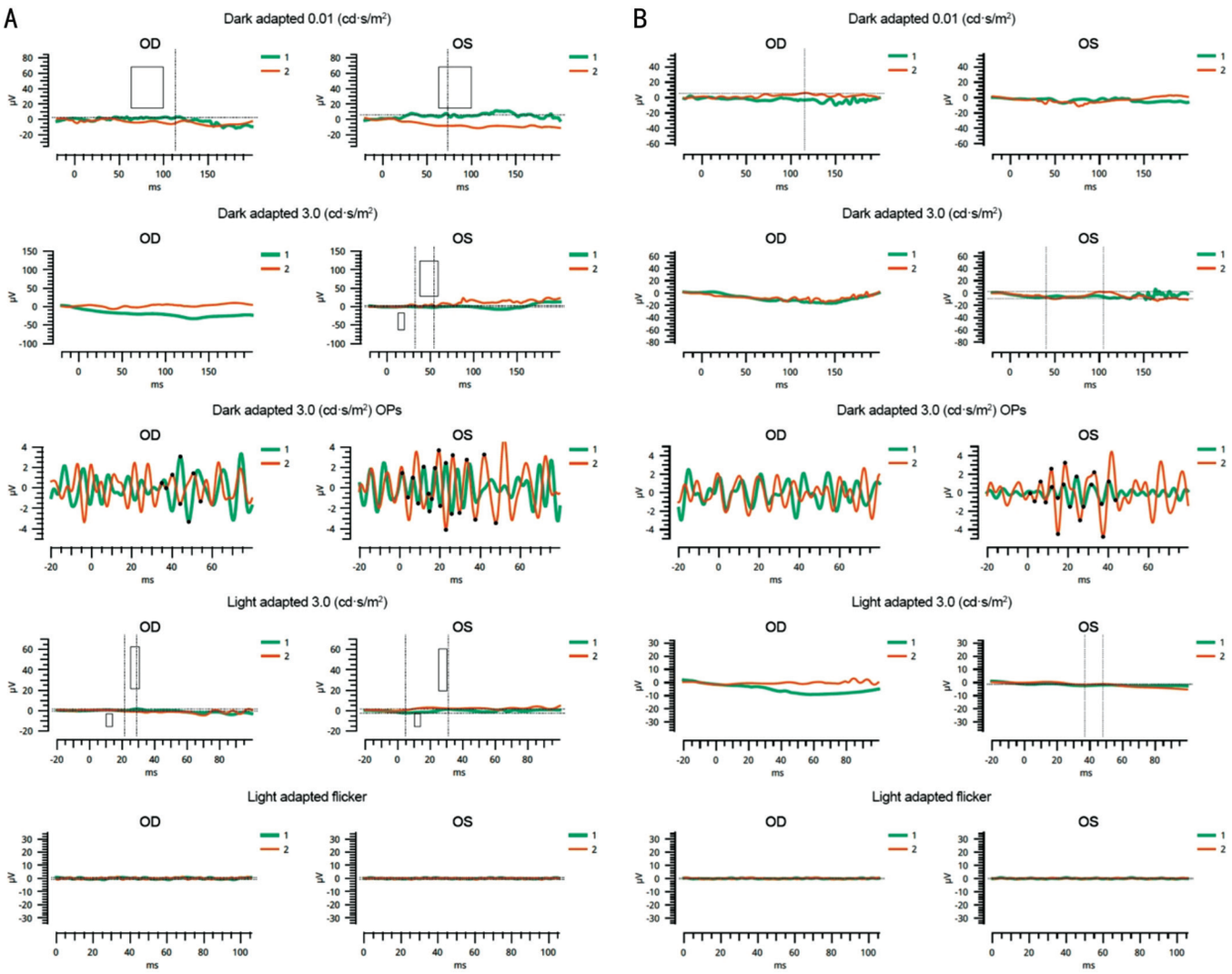

Figure 4 Electroretinograms A: Electroretinogram of the proband at the initial visit showed extinguished cone and rod responses in both eyes. The amplitude of the oscillatory potentials was grossly impaired in both eyes, and more severely impaired in the right eye. The implicit time was prolonged in the right eye. B: Electroretinogram of the youngest brother at the latest follow-up visit showed extinguished cone and rod responses in both eyes. The amplitude and implicit time of the oscillatory potentials was abnormal in both eyes. Green line 1 and red line 2 represent two repeated measurements.

Figure 5 Appearance of the teeth in the two affected siblings Color dental image of the proband's primary teeth at the initial visit showed AOB, staining in the upper teeth, and irregular dentition in the lower teeth (A1). At the latest follow-up visit, her permanent teeth showed thin of enamel and irregular dentition (A2). At the initial visit, the youngest brother showed AOB, thin of enamel, and pitting in the upper teeth (B1). At the latest follow-up visit, dentin color became apparent due to progressive enamel thinning (B2). AOB: Anterior open bite.

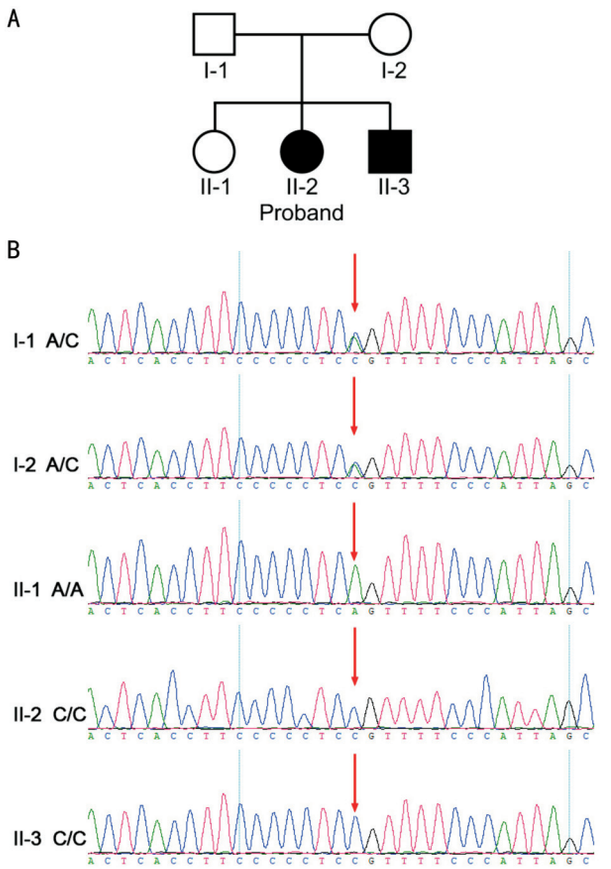

Figure 6 Pedigree and *CNNM4* variant of the JS family A: The pedigree of the JS family. B: Sanger sequencing chromatograms depicted the c.949A>C mutation in *CNNM4* in family members. Two patients (II-2 and II-3) carried the same homozygous variant (C/C), and their parents (I-1 and I-2) both carried the heterozygous variant (A/C). Red arrow indicates the variant. JS: Jalili syndrome.

with high genotypic and phenotypic heterogeneity between families. The rarity and high heterogeneity of JS make it easily be misdiagnosed with other hereditary retinal degenerations, such as Leber congenital amaurosis, cone degenerations, rod-cone dystrophy, achromatopsia, and a variety of isolated macular dystrophies. The most dominant difference between JS and other hereditary retinal degenerations is the dental abnormality. It reminds us of the importance of checking systemic abnormalities in patients with hereditary retinal degeneration, and genetic testing is needed for final conformation.

It has been reported that cones are initially affected with later rods involvement[37]. In our case, full-field ERG of the affected siblings showed extinguished cone and rod responses, indicating the involvement of both photoreceptors. This was in accordance with their manifestation of night blindness. The potential of OPs was impaired in both patients, indicating the dysfunction of amacrine and bipolar cells[18]. This was in line with a pathological study of JS, in which the inner retinal layers were partially affected with abnormal dendritic arborization in amacrine and bipolar cells[5].

In previously reported cases, the regions of high fluoride level in groundwater coincided with the regions of high frequency of JS[7]. Fluoride exposure might influence genomic stability and gene expression[40-41], and high fluoride concentration in groundwater might be an epigenetic factor in JS[42]. The fluoride concentration in groundwater of a town in Wuchuan had once been reported to be 1.5 mg/L[43], exceeding the 1.0 mg/L safety limit stipulated by China's standards for drinking-water quality (GB 5749-2022), while remaining within the upper threshold of the 1.5 mg/L safety level recommended by the WHO guidelines for drinking-water quality. The present reported family and their ancestors have been resided in Wuchuan. Hence, it is speculative that fluoride exposure might contribute to JS in this family.

We have summarized the visual acuities, basic characteristics, clinical features, and genetic mutations of JS from previous studies. By analyzing these reported cases, we found that the visual acuity level was positively associated with age, indicating that the visual acuity of JS patients deteriorated with aging. However, the longitudinal data from the current family showed no visual acuity change, because a 30-month observation period might not be long enough to validate the proposed age-related progression. A previous longitudinal study of seven patient with JS revealed structural and functional progression over time[4]. The correlation between visual acuity and age allowed us to predict the prognosis of vision and offer better advice for patients.

Red-tinted lenses are particularly beneficial for cone dystrophies as a low vision rehabilitation method. Red-tinted lenses can reduce photosensitivity and nystagmus by reducing the amount of short wavelength light reaching the retina and preventing rod photoreceptor saturation[44]. Besides the red tint, amber, brown, orangered, plum, and reddish brown all have been used successfully to reduce photosensitivity[45]. In addition, tinted lenses can improve the visual acuity, contrast sensitivity and color discrimination in children with cone dystrophies[46]. Therefore, patients with JS may experience symptomatic relief of photophobia with the aid of red-tinted lenses as well. They should also be advised of other low vision devices such as handheld telescope to improve their quality of life.

The current study has several limitations. First, the preliminary finding that visual acuity of JS patients deteriorated with aging was drawn from cross-sectional data in the literature and required replication in larger cohorts. Second, the longitudinal follow-up data on visual progression of the present cases failed to testify the correlation between age and vision due to the limited observation period.

In conclusion, the present study reported a novel homozygous missense variant c.949A>C (p.Ser317Arg) in *CNNM4*

Table 1 Summary of identified JS cases

Patient No.	Author (y)	Origin	Age (y)	Mutation	Domain	Snellen visual acuity	Mean logMAR visual acuity	Spherical equivalent (D)	Nystagmus	Color vision	Night vision	Photophobia	Fundus	Electroretinogram	Teeth
1	Michaelides *et al*[28] (2004); Parry *et al*[2] (2009)	Kosovo	8	c.1312 dupC; p.Leu438ProfsX9	CBS	3/60 OU	1.30	OD +6.50/-2.00×12; OS +6.00/-2.00×170	Fine pendular	Absent	Impaired	Marked	Bilateral macular atrophy and pigmentation	No detectable photopic cone responses. Rod function was markedly abnormal	Dysplastic and yellow/brown with almost no visible enamel
2	Michaelides *et al*[28] (2004); Parry *et al*[2] (2009)	Kosovo	10	c.1312 dupC; p.Leu438ProfsX9	CBS	3/60 OU	1.30	OD +4.50/-1.75×10; OS +4.50/-1.5×170	Fine pendular	Absent	Impaired	Marked	Bilateral macular atrophy and pigmentation	No detectable photopic cone responses. Rod function was markedly abnormal	Dysplastic and yellow/brown with almost no visible enamel
3	Polok *et al*[3] (2009)	Kosovo	14	c.1312dupC; p.L438ProfX9	CBS	20/200 OD 20/100 OS	0.85	Highly hyperopia	Pendular	-	-	Yes	Optic disk pallor, narrow vessels, macular atrophy with pigment mottling, and peripheral deep white dot deposits	-	Dysplastic and yellow and brown in color with no enamel layer and numerous carious lesions
4	Polok *et al*[3] (2009)	Kosovo	7	c.1312dupC; p.L438ProfX9	CBS	20/320 OU	1.20	Highly hyperopia	Pendular	-	-	Yes	Optic disk pallor, narrow vessels, macular atrophy with pigment mottling, and peripheral deep white dot deposits	-	Dysplastic and yellow and brown in color with no enamel layer and numerous carious lesions
5	Polok *et al*[3] (2009)	Unreported	6	c.971C>T; p.L324P	TM	10/200 OU	1.30	-	-	Impaired	-	-	-	-	Abnormal enamel
			38	c.971C>T; p.L324P	TM	LP OU		-	-	-	Night blind	-	Bilateral macular atrophy, bone spiculea in the midperiphery, optic atrophy	No response	Abnormal enamel
6	Jalili[6] (2010)	GazaB	5	c.1813C4T; p.Arg605X	CNMP	2/60	1.48	+2.00 to +4.00	Latent	Absent	Normal	Marked	Normal	Flicker: severely impaired	AI with AOB
7	Jalili[6] (2010)	GazaB	6	c.1813C4T; p.Arg605X	CNMP	5/60	1.08	+2.00 to +4.00	Fine pendular	Absent	Normal	Marked	Normal	Flicker: severely impaired	AI with AOB
8	Jalili[6] (2010)	GazaB	10	c.1813C4T; p.Arg605X	CNMP	6/60	1.00	+2.00 to +4.00	Fine pendular	Absent	Normal	Marked	Minor retinal epithelial defects	Flicker: severely impaired	AI with AOB
9	Doucette *et al*[29] (2013)	Northern Europe	28	c.1555C>T; p.R519X	Linker	20/300 OU	1.18	Myopia	Yes	Nil	-	-	-	Rod: borderline; cone: absent	Teeth extracted, severe enamel dysplasia
10	Doucette *et al*[29] (2013)	Northern Europe	19	c.1555C>T; p.R519X	Linker	20/200 OU	1.00	-	Yes	Nil	-	-	Maculopathy	-	Poor dentition and defective enamel
11	Doucette *et al*[29] (2013)	Northern Europe	16	c.1555C>T; p.R519X	Linker	20/200 OU	1.00	Myopia	Yes	Nil	-	-	-	-	Severe enamel dysplasia, irregular teeth with brown discoloration, marked wearing, jumbled eruption pattern
12	Luder *et al*[9] (2013)	Kosovo	5	c.1312dupC; p.L438ProfX9	CBS	20/200 OU	1.00	+8.00 to +9.00	-	-	-	Yes	Macular changes (bull's eye maculopathy) and a pale optic disc	-	Yellow-brown discolored with enamel hypoplasia
13	Luder *et al*[9] (2013)	Kosovo	2	c.1312dupC; p.L438ProfX9	CBS	20/200 OU	1.00	+8.00 to +9.00	Horizontal pendular-jerk	-	-	Yes	Macular changes (bull's eye maculopathy) and a pale optic disc	Reduced rod responses and nonrecordable cone responses	Yellow-brown discolored with enamel hypoplasia
14	Gerth-Kahlert *et al*[30] (2015)	Kosovo	15	c.1312dup; p.Leu438Profs*9	CBS	20/200 OU	1.00	-0.50 to +2.00	Fine pendular	-	-	-	Bull's eye maculopathy	Scotopic: reduced, delayed; photopic: not recordable	AI
15	Gerth-Kahlert *et al*[30] (2015)	Kosovo	16	c.1312dup; p.Leu438Profs*9	CBS	20/400 OU	1.30	-0.50 to +2.00	Fine pendular	-	-	-	Diffuse retinal dystrophy	Scotopic: reduced, delayed; photopic: not recordable	AI
16	Wang *et al*[31] (2015)	China	8	c.896_897insT; p.A300CfsX22	TM	0.1	1.00	Hyperopia	Yes	-	-	-	Macular atrophy with yellow appearance and scattered bone spicule pigmentation	Extinguished	AI
17	Rahimi-Aliabadi *et al*[32] (2016)	Iran	25	c.1091delG; I332FfsX10	TM	20/150 OD 20/120 OS	0.83	OD −0.75 OS −0.50	Latent	-	-	Yes	Mild macular atrophy, pigment clumps, attenuated vessels in mid-periphery	Scotopic: flat; Photopic: decreased amplitudes	AI
18	Rahimi-Aliabadi *et al*[32] (2016)	Iran	27	c.1091delG; I332FfsX10	TM	CF		OD +1.50/-2.00×50 OS +1.00/-1.50×140	Yes	-	-	Yes	Macular coloboma, pigment clumps, attenuated vessels	Scotopic: flat; photopic: flat	AI

Int J Ophthalmol, Vol. 18, No. 12, Dec. 18, 2025 www.ijo.cn
Tel: 8629-82245172 8629-82210956 Email: ijopress@163.com

Table 1 Summary of identified JS cases (continued)

Patient No.	Author (y)	Origin	Age (y)	Mutation	Domain	Snellen visual acuity	Mean logMAR visual acuity	Spherical equivalent (D)	Nystagmus	Color vision	Night vision	Photophobia	Fundus	Electroretinogram	Teeth
19	Rahimi-Aliabadi *et al*[32] (2016)	Iran	32	c.1091delG; I332FfsX10	TM	CF		OD +2.50/-4.00×180; OS +2.50/-4.00×180	Yes	-	-	Yes	Severe macular atrophy (beaten bronze), pigment clumps and diffuse whitish dots, attenuated vessels	Scotopic: flat; photopic: flat	AI
20	Rahimi-Aliabadi *et al*[32] (2016)	Iran	39	c.1091delG; I332FfsX10	TM	HM		OD +1.50/-1.50×180; OS +2.00/-1.50×180	Yes	-	-	Yes	Macular coloboma, pigment clumps, attenuated vessels	Scotopic: flat; photopic: flat	AI
21	Wawrocka *et al*[33] (2017)	Poland	25	c.1076T>C; p.(Leu359Pro)	CBS	HM		-	Yes	Absent	Impaired	Yes	Pale optic discs and round, dystrophic changes in the central maculae with pigment rearrangements	Extinguished photopic and scotopic responses	Hypoplastic, immature, or hypocalcified dental enamel
22	Wawrocka *et al*[33] (2017)	Poland	5	c.1076T>C; p.(Leu359Pro)	CBS	0.05-0.1		-	-	-	-	-	-		
23	Wawrocka *et al*[33] (2017)	Poland	20	c.1076T>C; p.(Leu359Pro)	CBS	CF/1.5 m		-	-	-	-	-	-		
24	Topçu *et al*[34] (2017)	Turkey	8	c.1781A>G; p.N594S	CNMP	20/200	1.00	+5.00 to +6 .00	-	-	Normal	Yes	Normal	Cone cells: no response; rod cells: impaired response	Hypoplastic–hypomineralized type
25	Topçu *et al*[34] (2017)	Turkey	12	c.1781A>G; p.N594S	CNMP	20/200	1.00	+5.00 to +6 .00	-	-	Normal	Yes	Normal	Cone cells: no response; rod cells: impaired response	Hypoplastic–hypomineralized type
26	Topçu *et al*[34] (2017)	Turkey	14	c.1781A>G; p.N594S	CNMP	20/200	1.00	+5.00 to +6 .00	-	-	Normal	Yes	Normal	Cone cells: no response; rod cells: impaired response	Hypoplastic–hypomineralized type
27	Hirji *et al*[4] (2018)	Kosovo	6	c.1312dupC; p.L438ProfX9	CBS	20/399 OU	1.30	-	Fine pendular	Absent	Impaired	Yes	Bilateral macular atrophy	No detectable cone ERGs, with markedly reduced rod function	Hypoplastic variant of AI
			21	c.1312dupC; p.L438ProfX9	CBS	HM		-	-	-		-	-	-	
28	Hirji *et al*[4] (2018)	Kosovo	4	c.1312dupC; p.L438ProfX9	CBS	20/399 OU	1.30	-	Fine pendular	Absent	Impaired	Yes	Bilateral macular atrophy	No detectable cone ERGs, with markedly reduced rod function	Hypoplastic variant of AI
			19	c.1312dupC; p.L438ProfX9	CBS	CF			-	-		-	-	-	-
29	Hirji *et al*[4] (2018)	Kosovo	5	c.1312dupC; p.L438ProfX9	CBS	20/200 OU	1.00	-	Yes	-	-	Yes	-	Cone-rod dystrophy	-
			15	c.1312dupC; p.L438ProfX9	CBS	20/126 OU	0.80	-	-	-	-	-		-	-
30	Hirji *et al*[4] (2018)	Pakistan	3	c.1226C>T; p.Pro409Leu	CBS	20/98 OU	0.69	-	Yes	-	-	Yes	Essentially normal, optic discs appeared slightly pale	-	-
			5	c.1226C>T; p.Pro409Leu	CBS	20/200 OD 20/252 OS	1.05	-	-	-	-	-	-	-	-
31	Hirji *et al*[4] (2018)	Afghanistan	7	c.C734T; p.Ser245Leu	TM	20/200 OU	1.00	-	Yes	-	-	Yes	-	-	Yellowish coloration
			45	c.C734T; p.Ser245Leu	TM	LP OU		-	-	-	-	-	Pale discs, severe macular atrophy, attenuated vessels, and peripheral retinal pigmentary changes	-	All removed and replaced with artificial dentition at 26y of age
32	Hirji *et al*[4] (2018)	Afghanistan	16	c.C734T; p.Ser245Leu	TM	20/317 OD 20/480 OS	1.29	-	Pendular	-	Nyctalopia	-	Bilateral macular atrophy with scalloped patchy deep retinal atrophy outside the arcades	Non-detectable rod and cone responses	-
			27	c.C734T; p.Ser245Leu	TM	20/1002 OD 20/796 OS	1.65	-	-	-	-	-	-	-	-
33	Maia *et al*[35] (2018)	Brazil	13	c.971T>C; p.Leu324Pro	TM	20/640 OD 20/1600 OS	1.70	+5.00	Pendular	Achromatopsia	-	Yes	Decreased macular reflex and macular pigmentation mobilization	Complete absence of cone and rod responses	Yellowish discoloration, rough surfaces and conspicuous and irregular defects
34	Li *et al*[10] (2018)	Amish	20	c.C1813T; p.R605X	CNMP	20/400 OU	1.30	-	-	-	-	-	Optic nerve and macular atrophy	-	All extracted, wearing dentures
35	Li *et al*[10] (2018)	Amish	17	c.C1813T; p.R605X	CNMP	6/200 OU	1.52	-	-	-	-	-	Optic nerve and macular atrophy	-	All extracted, wearing dentures

Table 1 Summary of identified JS cases (continued)

Patient No.	Author (y)	Origin	Age (y)	Mutation	Domain	Snellen visual acuity	Mean logMAR visual acuity	Spherical equivalent (D)	Nystagmus	Color vision	Night vision	Photophobia	Fundus	Electroretinogram	Teeth
36	Li *et al*[10] (2018)	Amish	24	c.C1813T; p.R605X	CNMP	2/200 OU	2.00	-		-	-	-	Optic nerve and macular atrophy	-	All extracted, wearing dentures
37	Prasov *et al*[36] (2020)	Guatemala	15	c.706C>T; p.Arg236Trp	TM	20/250 OD 20/200 OS	1.05	OD −2.75/+2.25×103; OS −3.00/+3.00×76	Yes	Absent	-	Yes	Bull's eye maculopathy and granular pigment changes in the periphery	Scotopic: reduced, delayed; Photopic: not recordable	Tooth decay, enamel absent
38	Prasov *et al*[36] (2020)	Guatemala	16	c.706C>T; p.Arg236Trp	TM	20/200 OD 20/160 OS	0.95	OD +1.00/+4.50×109; OS − 0.25/+4.25×69	Yes	Absent	-	-	Bull's eye maculopathy, perivascular and segmental pigment deposition in the inferior retina, and mild vascular attenuation	Scotopic: mildly reduced, delayed; Photopic: not recordable	Absence of enamel
39	Prasov *et al*[36] (2020)	Puerto Rico/ Caucasia	3	c.279delC; p.Phe93Leufs*31	ECD	20/360 OU	1.26	OD −3.25/+2.25×90; OS − 3.25 /+2.50×95	-	-	-	-	Diffuse granular pigment changes and bull's eye maculopathy	-	Yellow/opaque appearance of the anterior teeth with thinning or absence of enamel
40	Hyde *et al*[37] (2022)	Palestine	5	c.482 T > C; p.Leu161Pro	ECD	20/200 OD 20/400 OS	1.15	OD +1.50/+1.00×105; OS +1.25/+1.00×80	Yes	Color confusion	-	Yes	Normal	-	Generalized enamel defect
41	Hyde *et al*[37] (2022)	Palestine	14	c.482 T>C; p.Leu161Pro	ECD	20/200 OD 20/200 OS	1.00	OD +2.00×100; OS −0.50/+2.75×70	Yes	Dyschromatopsia	-	Yes	Bull's atrophic lesion of the macula with foveal hyperpigmentation	Cone: extinguished; rod: normal	Thin enamel, yellow-brown tooth discoloration and evidence of post-eruptive enamel breakdown, AOB and spacing between teeth
42	Hyde *et al*[37] (2022)	Palestine	15	c.482 T>C; p.Leu161Pro	ECD	20/100 OD 20/200 OS	0.85	OD −3.50/+2.75×95; OS −4.50/+2.25×75	Yes	Dyschromatopsia		Yes	Foveal hypopigmentation	Cone: extinguished; rod: normal	Thin, yellow-brown discolored enamel
43	Li *et al*[38] (2022)	China	45	c.598T>C; p.S200P	TM	LP OU		-	Yes	-	-	Yes	Diffused chorioretinal atrophy with a prominent macular coloboma	-	Full dental implant
44	Li *et al*[38] (2022)	China	40	c.598T>C; p.S200P	TM	LP OU		-	Yes	-	-	Yes	Diffused chorioretinal atrophy with a prominent macular coloboma	-	Dental decay, staining, irregular shapes, and loss of teeth
45	Khan[39] (2024)	United Arab Emirates	3	c.509T>C; p.Leu170Pro	ECD	20/400	1.30	+4.00	-	-	-	-	/	-	-
46	Franca *et al*[5] (2025)	Unreported	15	c.971T>C; p.Leu324Pro	TM	LP OU		-	-	-	-	Yes	Panretinal degeneration, including macular atrophy	-	Dental anomalies and full mouth extraction

AOB: Anterior open bite; AI: Amelogenesis imperfecta; CBS: Cystathionine-β-synthase; CF: Count fingers; CNMP: Cyclic nucleotide monophosphate binding-like; ECD: Extracellular domain; HM: Hand movement; JS: Jalili syndrome; LP: Light perception; TM: Transmembrane domain; OD: Oculus dexter; OS: Ocalus sinister; OU: Oculus uterque; ERG: Electroretinography.

Table 2 Visual acuity classification and corresponding age information in JS patients

Visual acuity level	Age (mean±SD, range, y)
Level 2: 6/60 to <6/18 (*n*=19)	11.74±5.91, 2-25
Level 3: 3/60 to <6/60 (*n*=17)	9.59±7.02, 3-28
Level 4: 1/60 or CF at 1 m to <3/60 (*n*=7)	20.00±9.36, 5-32
Level 5: LP to <1/60 or CF at 1 m (*n*=10)	31.20±11.29, 15-45
Total: *n*=53	15.81±11.23, 2-45

CF: Count fingers; JS: Jalili syndrome; LP: Light perception.

Int J Ophthalmol, Vol. 18, No. 12, Dec. 18, 2025 www.ijo.cn
Tel: 8629-82245172 8629-82210956 Email: ijopress@163.com

in a Chinese family with JS. The visual acuities, basic characteristics, clinical features, and genetic mutations of JS from previously reported papers have been summarized. The visual acuity of JS patients might deteriorate with aging.

ACKNOWLEDGEMENTS

Foundation: Supported by Shenzhen Science and Technology Program, Shenzhen, China (No.JCYJ20210324134004013).

Conflicts of Interest: Lu J, None; **Liang SY,** None; **Li Z,** None; **Gan R,** None; **Cheng XR,** None; **Chen QS,** None.

REFERENCES

1 Jalili IK, Smith NJ. A progressive cone-rod dystrophy and amelogenesis imperfecta: a new syndrome. *J Med Genet* 1988;25(11):738-740.

2 Parry DA, Mighell AJ, El-Sayed W, *et al*. Mutations in CNNM4 cause Jalili syndrome, consisting of autosomal-recessive cone-rod dystrophy and amelogenesis imperfecta. *Am J Hum Genet* 2009;84(2):266-273.

3 Polok B, Escher P, Ambresin A, *et al*. Mutations in CNNM4 cause recessive cone-rod dystrophy with amelogenesis imperfecta. *Am J Hum Genet* 2009;84(2):259-265.

4 Hirji N, Bradley PD, Li SN, *et al*. Jalili syndrome: cross-sectional and longitudinal features of seven patients with cone-rod dystrophy and amelogenesis imperfecta. *Am J Ophthalmol* 2018;188:123-130.

5 Franca M, Providência J, Castela G, *et al*. Clinical and histopathologic findings in jalili syndrome. *Ophthalmol Retina* 2025;9(5):476-483.

6 Jalili IK. Cone-rod dystrophy and amelogenesis imperfecta (Jalili syndrome): phenotypes and environs. *Eye (Lond)* 2010;24(11):1659-1668.

7 Daneshmandpour Y, Darvish H, Pashazadeh F, *et al*. Features, genetics and their correlation in Jalili syndrome: a systematic review. *J Med Genet* 2019;56(6):358-369.

8 Yamazaki D, Funato Y, Miura J, *et al*. Basolateral Mg^{2+} extrusion *via* CNNM4 mediates transcellular Mg^{2+} transport across epithelia: a mouse model. *PLoS Genet* 2013;9(12):e1003983.

9 Luder HU, Gerth-Kahlert C, Ostertag-Benzinger S, *et al*. Dental phenotype in jalili syndrome due to a c.1312 dupC homozygous mutation in the CNNM4 gene. *PLoS One* 2013;8(10):e78529.

10 Li SS, Xi QS, Zhang XY, *et al*. Identification of a mutation in CNNM4 by whole exome sequencing in an Amish family and functional link between CNNM4 and IQCB1. *Mol Genet Genomics* 2018;293(3):699-710.

11 Shahsavan A, Lee EL, Illes K, *et al*. Dimerization of the CNNM extracellular domain. *Protein Sci* 2024;33(2):e4860.

12 Hirata Y, Funato Y, Takano Y, *et al*. Mg^{2+}-dependent interactions of ATP with the cystathionine-β-synthase (CBS) domains of a magnesium transporter. *J Biol Chem* 2014;289(21):14731-14739.

13 Giménez-Mascarell P, Oyenarte I, González-Recio I, *et al*. Structural insights into the intracellular region of the human magnesium transport mediator CNNM4. *Int J Mol Sci* 2019;20(24):6279.

14 Chen YS, Kozlov G, Fakih R, *et al*. Mg^{2+}-ATP sensing in CNNM, a putative magnesium transporter. *Structure* 2020;28(3):324-335.e4.

15 Chen YS, Kozlov G, Fakih R, *et al*. The cyclic nucleotide-binding homology domain of the integral membrane protein CNNM mediates dimerization and is required for Mg^{2+} efflux activity. *J Biol Chem* 2018;293(52):19998-20007.

16 Chen YS, Kozlov G, Moeller BE, *et al*. Crystal structure of an archaeal CorB magnesium transporter. *Nat Commun* 2021;12:4028.

17 Kato K, Kondo M, Sugimoto M, *et al*. Effect of pupil size on flicker ERGs recorded with RETeval system: new mydriasis-free full-field ERG system. *Invest Ophthalmol Vis Sci* 2015;56(6):3684-3690.

18 Zhang T, Lu JL, Jiang ZX, *et al*. The development of electroretinographic oscillatory potentials in healthy young children. *J Clin Med* 2022;11(19):5967.

19 Robson AG, Frishman LJ, Grigg J, *et al*. ISCEV Standard for full-field clinical electroretinography (2022 update). *Doc Ophthalmol* 2022;144(3):165-177.

20 Zhang T, Lu JL, Sun LM, *et al*. Mydriasis-free flicker electroretinograms in 204 healthy children aged 0-18y: reference data from two cohorts. *Transl Vis Sci Technol* 2021;10(13):7.

21 Grace SF, Lam BL, Feuer WJ, *et al*. Nonsedated handheld electroretinogram as a screening test of retinal dysfunction in pediatric patients with nystagmus. *J AAPOS* 2017;21(5):384-388.

22 Anslan S, Mikryukov V, Armolaitis K, *et al*. Highly comparable metabarcoding results from MGI-Tech and Illumina sequencing platforms. *PeerJ* 2021;9:e12254.

23 Wei XM, Ju XC, Yi X, *et al*. Identification of sequence variants in genetic disease-causing genes using targeted next-generation sequencing. *PLoS One* 2011;6(12):e29500.

24 Li H, Durbin R. Fast and accurate short read alignment with Burrows-Wheeler transform. *Bioinformatics* 2009;25(14):1754-1760.

25 Richards S, Aziz N, Bale S, *et al*. Standards and guidelines for the interpretation of sequence variants: a joint consensus recommendation of the American College of Medical Genetics and Genomics and the Association for Molecular Pathology. *Genet Med* 2015;17(5):405-424.

26 Lee JH, Park SH, Yim JS, *et al*. The first Korean child of jalili syndrome with a novel missense mutation in cation transport mediator 4 (CNNM4): a case report. *Korean J Ophthalmol* 2023;37(2):195-197.

27 Jackson ML, Virgili G, Shepherd JD, *et al*. Vision rehabilitation preferred practice pattern®. *Ophthalmology* 2023;130(3):P271-P335.

28 Michaelides M, Bloch-Zupan A, Holder GE, *et al*. An autosomal recessive cone-rod dystrophy associated with amelogenesis imperfecta. *J Med Genet* 2004;41(6):468-473.

29 Doucette L, Green J, Black C, *et al*. Molecular genetics of Achromatopsia in Newfoundland reveal genetic heterogeneity, founder effects and the first cases of Jalili syndrome in North America. *Ophthalmic Genet* 2013;34(3):119-129.

30 Gerth-Kahlert C, Seebauer B, Dold S, *et al*. Intra-familial phenotype variability in patients with Jalili syndrome. *Eye* (*Lond*) 2015;29(5):712-716.

31 Wang H, Wang X, Zou X, *et al*. Comprehensive molecular diagnosis of a large Chinese leber congenital amaurosis cohort. *Invest Ophthalmol Vis Sci* 2015;56(6):3642-3655.

32 Rahimi-Aliabadi S, Daftarian N, Ahmadieh H, *et al*. A novel mutation and variable phenotypic expression in a large consanguineous pedigree with Jalili syndrome. *Eye* (*Lond*) 2016;30(11):1424-1432.

33 Wawrocka A, Walczak-Sztulpa J, Badura-Stronka M, *et al*. Co-occurrence of Jalili syndrome and muscular overgrowth. *Am J Med Genet A* 2017;173(8):2280-2283.

34 Topçu V, Alp MY, Alp CK, *et al*. A new familial case of Jalili syndrome caused by a novel mutation in CNNM4. *Ophthalmic Genet* 2017;38(2):161-166.

35 Maia CMF, Machado RA, Gil-da-Silva-Lopes VL, *et al*. Report of two unrelated families with Jalili syndrome and a novel nonsense heterozygous mutation in CNNM4 gene. *Eur J Med Genet* 2018;61(7):384-387.

36 Prasov L, Ullah E, Turriff AE, *et al*. Expanding the genotypic spectrum of Jalili syndrome: Novel CNNM4 variants and uniparental isodisomy in a North American patient cohort. *Am J Med Genet A* 2020;182(3):493-497.

37 Hyde RA, Kratunova E, Park JC, *et al*. Cone pathway dysfunction in Jalili syndrome due to a novel familial variant of *CNNM4* revealed by pupillometry and electrophysiologic investigations. *Ophthalmic Genet* 2022;43(2):268-276.

38 Li HJ, Huang YF, Li J, *et al*. Novel homozygous nonsynonymous variant of CNNM4 gene in a Chinese family with Jalili syndrome. *Mol Genet Genomic Med* 2022;10(3):e1860.

39 Khan AO. The genetic basis of clinically suspected Achromatopsia in the united Arab emirates. *Retina* 2024;44(11):2019-2025.

40 Everett ET. Fluoride's effects on the formation of teeth and bones, and the influence of genetics. *J Dent Res* 2011;90(5):552-560.

41 Garcia ALH, de Souza MR, Picinini J, *et al*. Unraveling gene expression and genetic instability in dental fluorosis: investigating the impact of chronic fluoride exposure. *Sci Total Environ* 2024;906:167393.

42 Ravi M, Karthikeyan PD, Tewari N, *et al*. Dentofacial manifestations in a child with Jalili syndrome. *Spec Care Dentist* 2024;44(4):1026-1035.

43 Wu JQ, Chen ZC, Chen PJ, Zhao JX. Epidemiological study on endemic fluorosis in Guangdong Province. *Journal of Tropical Medicine* 2001;1(2):181-187.

44 Vincent SJ. The use of contact lenses in low vision rehabilitation: optical and therapeutic applications. *Clin Exp Optom* 2017;100(5):513-521.

45 Schornack MM, Brown WL, Siemsen DW. The use of tinted contact lenses in the management of Achromatopsia. *Optometry* 2007;78(1):17-22.

46 Rajak SN, Currie AD, Dubois VJ, *et al*. Tinted contact lenses as an alternative management for photophobia in stationary cone dystrophies in children. *J AAPOS* 2006;10(4):336-339.